Hindawi
Geofluids
Volume 2021, Article ID 6650616, 20 pages
https://doi.org/10.1155/2021/6650616

Research Article

Laboratory Investigation on the Effects of Natural Fracture on Fracture Evolution of Granite Exposed to Freeze-Thaw-Cyclic (FTC) Loads

Yu Wang, Xuefeng Yi, Shaohua Gao, and Hao Liu

Beijing Key Laboratory of Urban Underground Space Engineering, Department of Civil Engineering, School of Civil & Resource Engineering, University of Science & Technology Beijing, Beijing 100083China

Correspondence should be addressed to Yu Wang; wyzhou@ustb.edu.cn

Received 2 December 2020; Revised 20 December 2020; Accepted 26 December 2020; Published 9 January 2021

Academic Editor: Zhigang Tao

The natural fractures in rock mass are susceptible to damage evolution when subjecting to repeated freeze-thaw (F-T) weathering in cold regions, which can lead to the instability of rock engineering and even occurrence of geological hazards. Knowledge of how natural fracture impacts the overall fracture evolution of freeze-thawed rock is important to predict the stability of rock structure. In this work, we reported uniaxial experimental measurements of the changes in strength, deformation, acoustic emission (AE) pattern, and Felicity effect during increasing amplitude stress-cycling conditions on granite. The results show that the change of fracture aperture is related to the fracture openness and filling characteristics, open-type fracture is sensitive to F-T treatment, and its aperture increases faster than the close-type and fill-type fracture. In addition, strength decreases, and the damping characteristics first decrease and then increase with increasing natural fracture volume. AE activities also present different responses during sample deformation. The proportion of AE signals having low-frequency characteristics increases with increasing natural fracture volume, and the shear sliding along natural fracture results in the surge of AE activities. Moreover, the Felicity effect indicates that the Felicity ratio presents a fluctuation decreasing trend, and the preexisting fractures alter the stress memory characteristics of rock. It is suggested that the changes of the geomechanical and AE pattern are the interactions between the natural fracture and the newly stimulated fracture. The testing results are expected to improve the understanding of the influence of natural fractures on rock fracture evolution and can be helpful to predict the stability of rock structures and rock mass in cold regions.

1. Introduction

Freeze-thaw (F-T) weathering frequently occurs in cold regions, and it leads to the deterioration of rock geomechanical properties, therefore severely impacts the stability of rock engineering and even inducing geological hazards. For rock mass containing structure planes, often named as natural fracture, the water migration and water-ice phase transformation in the preexisting fractures are stronger than the intact rock. The preexisting cracks or discontinuities have a significant effect on the deformation, strength, and crack coalescence. Especially, under F-T conditions, a 9% volumetric expansion occurs when water turns to ice [1–5], and frost heaving pressure would produce within the natural fractures. The frost heaving pressure further drives the propagation of natural fractures, resulting in the increment of fracture aperture and length, and deteriorates the rock structure. In cold regions, the existing of natural fractures in rock structure is much more dangerous than in the normal thermoneutral condition. Therefore, it is of great importance to investigate the mechanical properties of naturally fractured rock in cold regions.

To simulate the field F-T condition for rock, F-T test is usually to be used to mimic the natural weathering of rock under low temperature at a faster place in the laboratory. The impacts of rock mineral composition, rock porosity, F-T cycle number, freeze temperature, F-T solution, etc., on rock mechanical properties have performed systematic

research, and corresponding damage models have been proposed to describe the F-T fatigue damage, mainly including the uniaxial compressive strength (UCS), elastic modulus, porosity, P- or S- velocities, and mass loss rate [3, 6–8]. Nowadays, plenty of devotions have also been done to investigate the F-T mechanical and physical properties of various kinds rock, such as dolomitic limestone [9], oil shale [10], diorite [11], tuff [12], sandstone [13, 14], granite [15], coal [16], mudstone [17], sandy mudstone [18], and slate [19] from various cold regions in China using various F-T laboratory tests. However, most of the investigations are focused on intact rock, and the effects of water-ice phase transformation on natural fractures and the frost heaving cracking have not been well understood. Huang et al. [19] proposed a coupled thermohydromechanical model to investigate the frost heaving strain in the preexisting flaws, and the influences of temperature and pore water/ice pressure on frost heaving strain have been studied. Huang et al. [20] conducted a laboratory testing on rock-like material containing single flaw under F-T and uniaxial compression, and the crack propagation characteristics and the frost heaving cracking behavior were studied. Lu et al. [21] conducted triaxial compression test on sandstone containing single flaw subjected to F-T treatment, and they considered the influences of confining pressure, F-T action, and loading on the deterioration of rock mechanical properties. Zhou et al. [22] studied the effect of F-T cycles in the cracking behavior of sandstone containing two unparallel preflaws under uniaxial compression, and the cracking process was recorded by high-speed digital video camera, and their investigations proved that the F-T damage characteristic of fractured rock is totally from the intact rock. For the F-T mechanical behaviors of fractured rock, most of them are applied to conventional uniaxial or triaxial stress paths. Actually, the freeze-thawed rocks are often subjected to complicated stress paths in cold regions. Especially for rock in the open pit mine slope, the excavation, blast vibration acts on rock mass, and the loading type is different from the conventional uniaxial or triaxial stress [23–26]. Generally, the stress disturbance loading is equivalent to cyclic loading, and loading and unloading experiments have been widely done on rock at room temperature. For the rock after F-T treatment, little literatures can be found about the mechanical behavior of rock under cyclic loading conditions.

The basic objective of the present work is to investigate the mechanical and emission acoustic characteristic of naturally fractured granite obtained from a high altitude and high cold open pit slope, in Xinjiang province, northwest of China. Rock samples having different natural fracture volumes were obtained by vertical coring on rock blocks. First, the rock samples were subjected to F-T treatment and then increasing amplitude stress-cycling experiments were conducted to investigate the changes of rock strength, deformation, acoustic emission pattern, and Felicity effect. The AE parameter and spectral analysis are used to reveal the crack initiation, propagation, and coalescence, and Felicity effect analysis is used to reveal the influence of natural fracture on the stress memory effect. This work is focused on revealing the effects of the preexisting natural fracture on the geomechanical and AE characteristics, and the results are helpful to understand the deterioration mechanism of naturally fractured rock mass in cold regions.

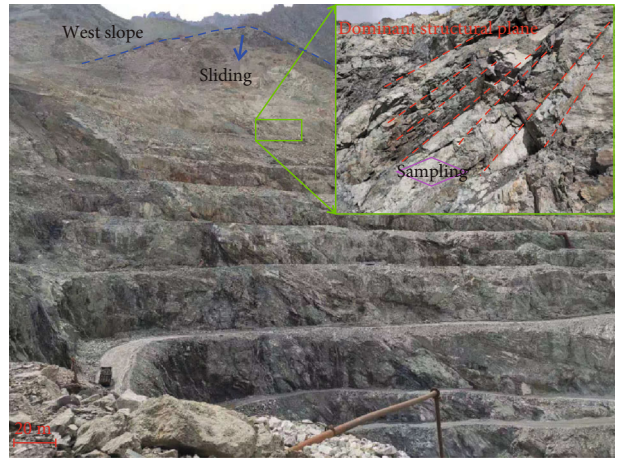

Figure 1: Result of the rock core from the west slope of Beizhan open pit slope. A set of dominant structural plane can be observed as drawn in red color.

2. Experimental Material and Methodology

2.1. Rock Material and Sample Preparation. The studied rock material was obtained from the Hejing Beizhan open pit slope located at the Xinjiang province, northwest of China. The lithology of the rock is granite, which is distributed at the west boundary of the open pit slope, as shown in Figure 1. A dominant structural plane can be clearly observed on the slope, which controls the stability of the open pit slope. The rock mass structural plane has an inclination of 290° and a dip angle of 70°.

From the results of X-ray powder diffraction (XRD), the granite was mainly composed of albite (75%), quartz (10%), magnesiohornblende (12%), orthoclase (8%), and biotite (13%) minerals. By scanning electron microscope imaging analysis (Figure 2), it can be seen that some microcracks develop at the interfaces of minerals; in addition, some large pores and plenty of small pores can be observed during the formation of granite. Samples of all the rocks tested were cored to a diameter of 50 mm and ground flat and parallel within ±0.1 mm to a nominal length of 100 mm according to the ISRM suggested method. Typical granite samples with natural fracture tested in this study are shown in Figure 3. It can be seen that the samples tested have natural fractures within them, and structural plane has similar orientation, which is parallel to the natural rock mass structural plane.

2.2. Experimental Device and Method. Before conducting static cyclic loading test, the samples were subjected to F-T treatment. First, the samples were conducted vacuum saturation for 24 hours. Then, a JS-DW-40 ultra-low temperature freezer was used to realize F-T cycles. According to the temperature changes of the Hejing Beizhan mining pit, in the F-T treatment, saturated samples were placed into the F-T

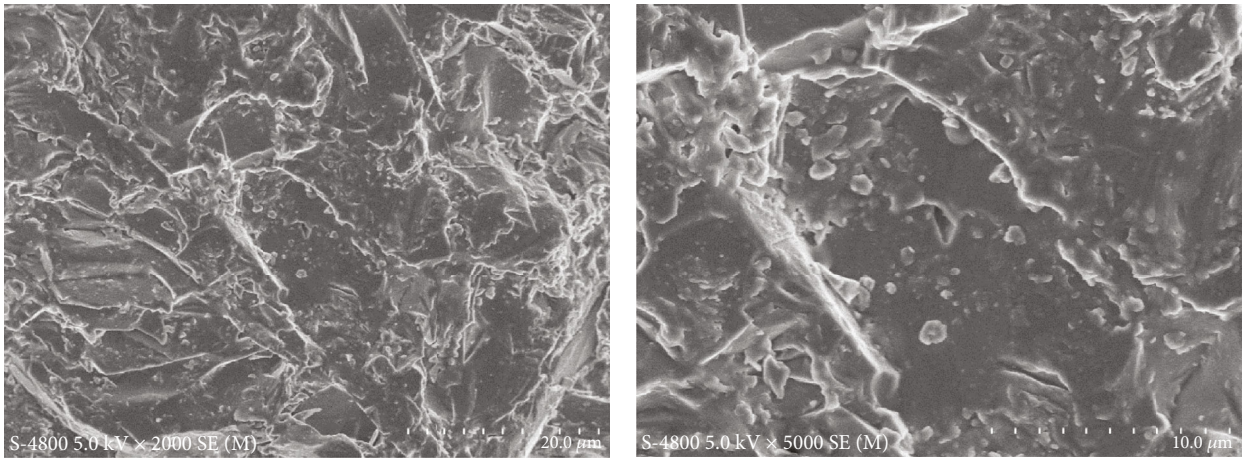

(a) (b)

Figure 2: SEM results for granite with different magnifications. (a, b) Plots of the SEM results with magnifications of 2000 and 5000 times, respectively.

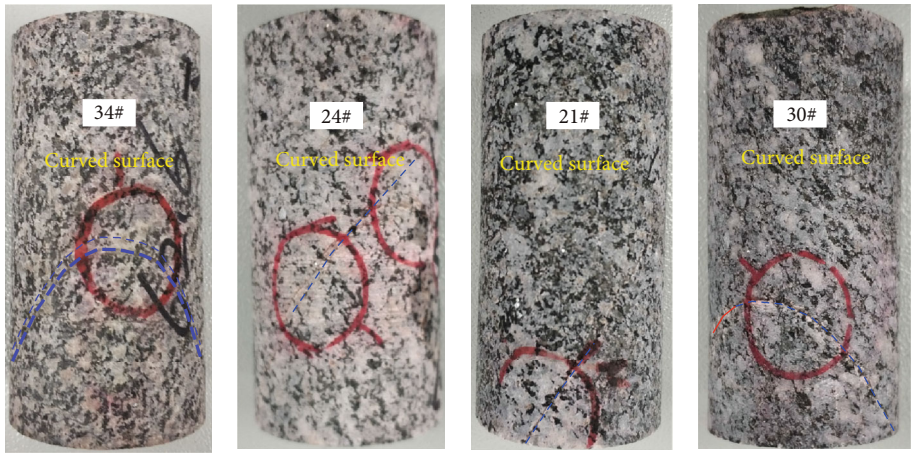

(a) (b) (c) (d)

Figure 3: Typical granite samples used in the increasing amplitude stress-cycling experiments. The natural fractures are schemed in blue color on the curved surface.

apparatus and adjusted 8 h for −40°C, and then the samples were removed from the freezer and placed into the water at 20°C, where they were allowed to thaw for a duration of 8 h, as shown in Figure 4. Under freeze condition, the whole sample containing the natural fractures was wrapped with cotton cloth in order to ensure the full freeze state, in order that the frost heaving force can act on the natural fractures. Here, four groups of samples containing natural fractures were treated with cyclic F-T treatment. A maximum F-T cycle of 120 times was applied to the naturally fractured granite samples.

All mechanical experiments were performed in a servo-controlled, triaxial rock mechanic testing system (GCTS RTR 2000). The axial and lateral strains were continuously monitored throughout each testing using LVDT displacement transducers. The fracture process was also continuously recorded by a PAC AE monitoring system (Figure 5; see also Wang et al. [27] for full details of the experimental configuration). Two AE sensors were used and installed at the positions of 40 mm and 60 mm from the bottom of rock sample and mounted on opposite positions. The AE sensors were bundled using a narrow piece of plastic wrap. A couplant,

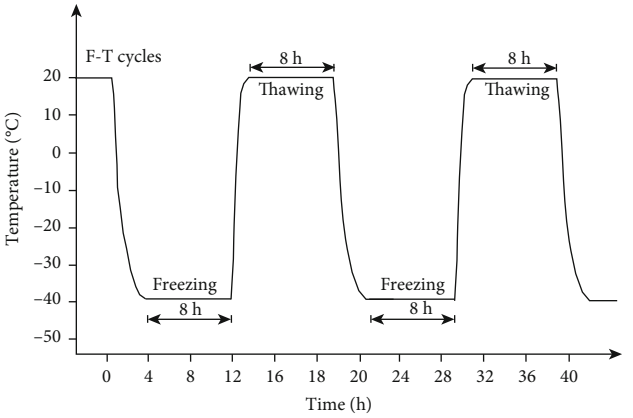

Figure 4: Freeze-thaw testing scheme for the granite samples.

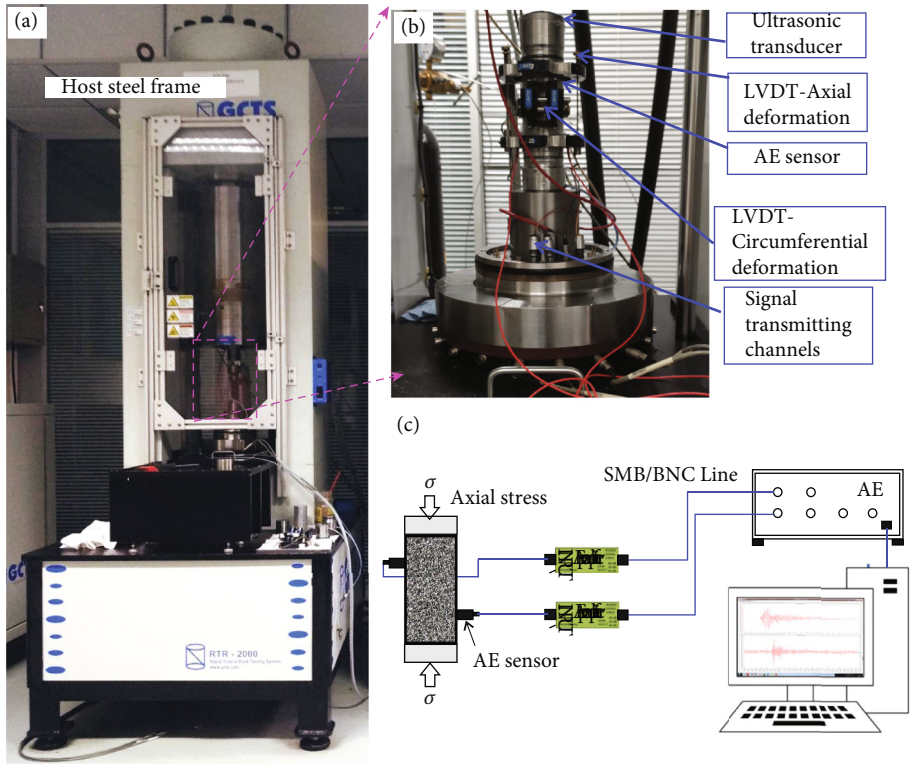

Figure 5: The testing system used for the increasing amplitude stress-cycling experiment ((a) GCTS 2000 rock mechanics machine, (b) LVDT system, and (c) scheme of AE system).

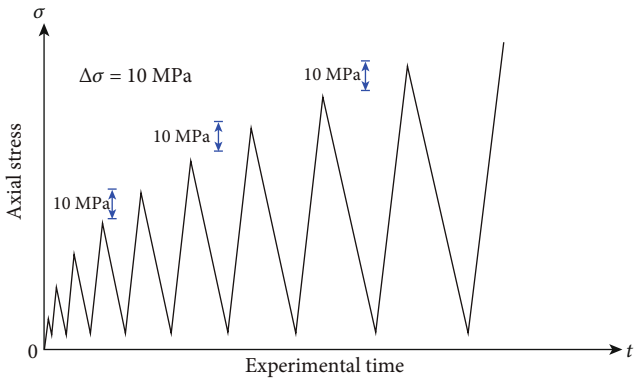

Figure 6: Scheme of the cyclic loading path for increasing amplitude stress-cycling tests.

vaseline, was employed between the sensors and the rock sample surfaces to ensure perfect contact. In the first cycle during increasing amplitude stress-cycling experiments, samples were loaded to a maximum stress of 20 MPa at a constant strain rate 0.06 mm/min (i.e., 1.0×10^{-6} s^{-1}) and then unloaded at half of loading rate (i.e., 0.03 mm/min) to 10 MPa. In each subsequent cycle, the maximum stress was increased by 10 MPa and samples again unloaded to 10 MPa. Stress cycling was continued in this way until all samples eventually failed. The testing stress path is plotted in Figure 6. Two groups of samples were tested; in group I, they experienced monotonous uniaxial loading; in group II, they are subjected to increasing amplitude stress-cycling conditions, as listed in Table 1.

3. Experimental Results and Analysis

3.1. Fracture Aperture Evolution Analysis. For the tested granite samples, three kinds of natural fracture can be observed from the rock surface, i.e., open type, close type, and fill type, and the fill-type fracture is filled with the mineral of calcite. Taking four rock samples of NFG-34#, FG-24#, NFG-21#, and NFG-30#, for example, close-type fracture can be found in sample 34#, open-type fractures can be found in samples 24# and 21#, and filled-type fracture was observed on the surface of 30#, as shown in Figure 7. During cyclic F-T treatment, as the fracture is saturated by water, frost heaving force generates when water transfers to ice, and the width of fracture changes with F-T cycles. Due the difference among the fracture physical characteristics, the evolution of fracture width F-T cycles may be different.

All the samples were subjected to 120 F-T cycles, for the three typical kinds of fracture (i.e., open, close, and fill), and the evolution of fracture width with F-T number is plotted in Figure 8. In order to reveal the relationship between fracture width and cyclic F-T number, power ($y = ax^b$), linear ($y = ax + b$), polynomial ($y = ax^2 + bx + c$), exponential ($y = ae^{bx}$), and logarithmic ($y = a + blnx$) regression fitting methods were executed, and the regression equations that have the largest correlation coefficient were finally determined. For the closed-type fracture, linear equation has the highest correlation coefficient, and it is used to fit the relationship between fracture width and F-T cycle. Also, it can be seen that the relationships between the open-type fracture, fill-type fracture, and F-T number obey to

Table 1: Testing scheme for the naturally fractured granite under uniaxial cyclic conditions.

Testing group	Sample ID	$L \times d$ (mm × mm)	Ms1 (g)	Ms2 (g)	Mass loss rate (%)	Initial damage degree (%)	Loading and unloading conditions
I	IG-1	100.07 × 49.06	572.3	/	0.13%	0	Uniaxial, monotonous compression, 0.06 mm/min
	IG-2	100.01 × 49.62	568.6	/	0.11%	0	
	IG-3	99.58 × 49.30	570.6	/	0.15%	0	
II	NFG-34	100.01 × 50.21	565.6	562.6	0.53%	0.19%	Uniaxial cyclic, static loading, loading rate 0.06 mm/min, unloading rate 0.03 mm/min; increasing amplitude stress of 10 MPa
	NFG-24	99.85 × 50.05	559.8	557.3	0.42%	0.15%	
	NFG-21	100.12 × 49.63	564.1	562.1	0.37%	0.13%	
	NFG-30	100.22 × 49.85	552.3	550.6	0.31%	0.11%	

Note: the initial damage degree of the samples was defined as the ratio of natural fracture volume to the sample volume.

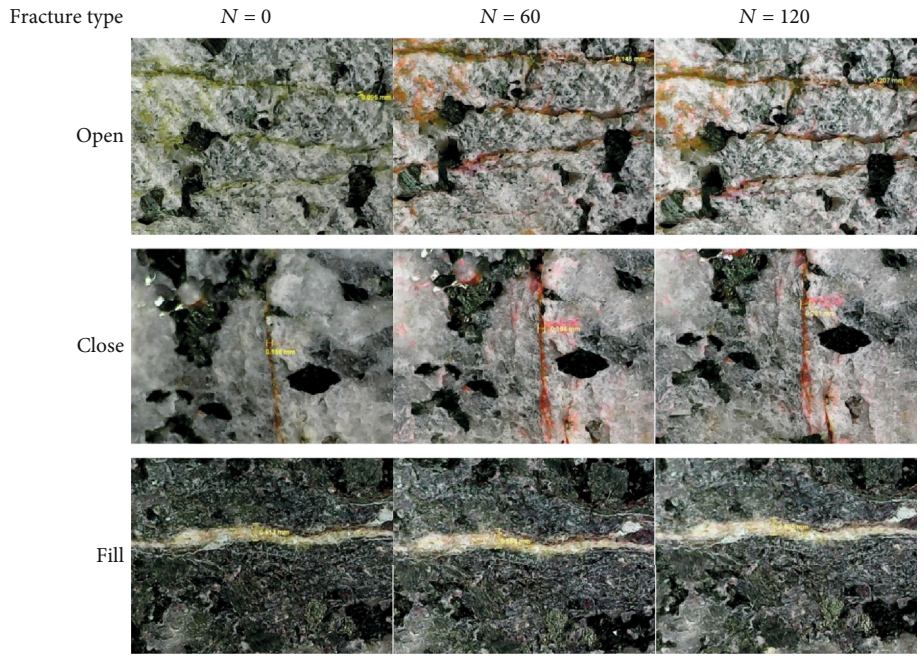

Figure 7: Fracture aperture changes with increasing F-T cycles. Three kinds of typical fracture of primary structural plane of open type, close type, and filled type were observed by the digital microscope.

exponential and polynomial equations. The fitting results show that the increasing rate of fracture width is the largest for the open-type fracture, and this implies that rock structure with open-type fracture is easy to be degraded. The existing of this kind of fracture is the most dangerous to the stability of rock mass.

3.2. Cyclic Stress Strain Response. For the tested samples, static and cyclic loading with increasing stress amplitude was applied to rock samples until failure. Reprehensive stress strain curves from the experiments on naturally fractured granite are given in Figure 9. It shows that the number of loading cycle is different for the four samples due to the difference of initial damage degree. The loading cycle number for the four tested sample is 5, 6, 7, and 9, respectively. The cycle number increases with decreasing the original fracture volume, and this result indicates that the ability to resist external loading decreases as the initial fracture volume increases.

The experimental data indicates that each successive loading cycle produced a change in the stress strain response of rock. The changes observed for the four tested rock are different which is impacted by the initial fracture scale in the rock. After multiple loading cycles, the samples failed eventually, and it is not the typical splitting failure like intact rock; the failure is controlled by the preexisting weak plane. We observed that NFG-30 is significantly stronger than other granite, with a peak stress of approximately 96.17 MPa as against 58.66 MPa for NFG-34, 61.82 MPa for NFG-24, and 73.05 MPa for NFG-21. Interested is that the morphology of the load-time curve at the failure point is different; oscillatory failure occurs for the samples having original fracture volume of 0.19% and 0.15%; sudden failure occurs for the samples having original fracture volume of 0.13% and 0.11%. The morphology of the stress strain curves at the post-peak stage reflects the failure mode, and the reason for the oscillatory pattern may be the sliding of rock block along the preexisting naturally fracture; the sudden drop pattern

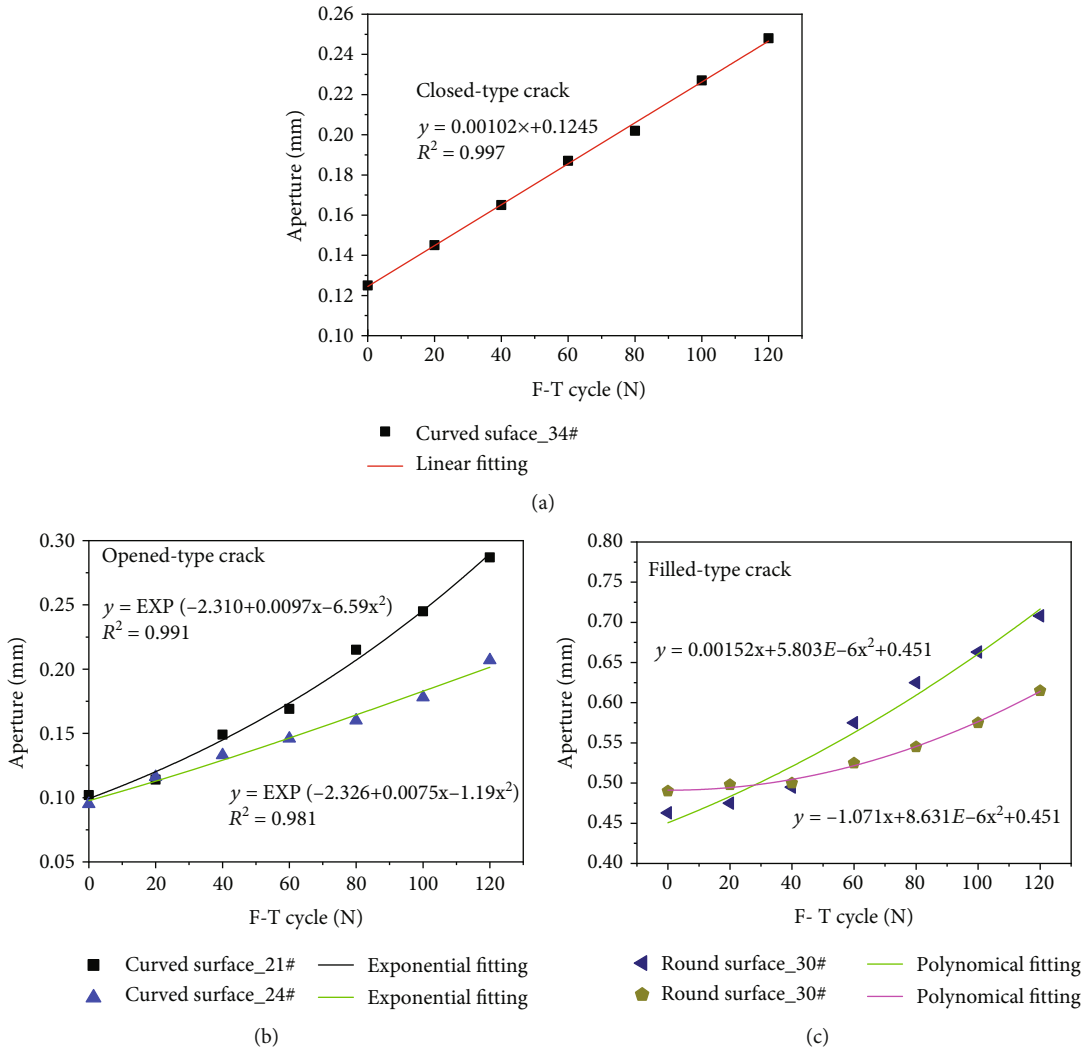

Figure 8: Depict of the changes of natural fracture aperture with F-T cycles. (a) Closed-type natural fracture; (b) opened-type natural fracture; (c) filled-type natural fracture.

may be the fracturing along the rock matrix. From the cyclic stress strain curve, the loading curve is not overlapped with the unloading curve, and hysteresis loops form during sample deformation. The formation of hysteresis loop indicates the occurrence of irreversible plastic deformation. It can also be seen that the morphology of hysteresis loop presents a sparse, dense, and sparse pattern, and the area of the hysteresis loop increases with sample deformation, and the increasing rate grows. Due to the preexisting natural fractures, it can be seen that the axial deformation is less than the lateral deformation, and the associated volumetric deformation becomes larger and larger. The changes of volumetric strain are mainly caused by the variation of lateral strain. Due to the influence of the preexisting fracture, the curve morphology at the postpeak stage is different. A gradual drop pattern is for the samples with larger natural fractures, and sudden drop pattern is for the samples with relatively small natural fracture.

3.3. Cyclic Deformation Characteristics. The axial, lateral, and volumetric deformations increase with experimental time during cyclic loading, as plotted in Figure 10. Partial deformation cannot restore with the increase of loading cycle, and the irreversible deformation increases with increasing cycle number. It can be seen that the axial strain shows regular triangle shape, and this implies that unloading strain rate is almost the same to the loading strain rate. However, the cyclic lateral strain curves show that the unloading rate is less than the loading rate, and the lateral deformation is relatively small compared to the axial deformation. The volumetric strain curves at the loading and unloading stage show obvious difference, and it is mainly influenced by the cyclic lateral strain; the unloading strain rate is also smaller than the axial unloading rate. The accumulated damage in rock results in the increment of volumetric expansion and the finial failure.

The irreversible deformation of the rock is calculated at each cycle, and Figure 11 shows the relationship between them and cycle number. The axial, lateral, and volumetric irreversible deformations all increase with increasing cycle number. It can be seen that the natural fracture position and aperture also affect the axial and lateral deformations, and no obvious change rule can be obtained for the tested

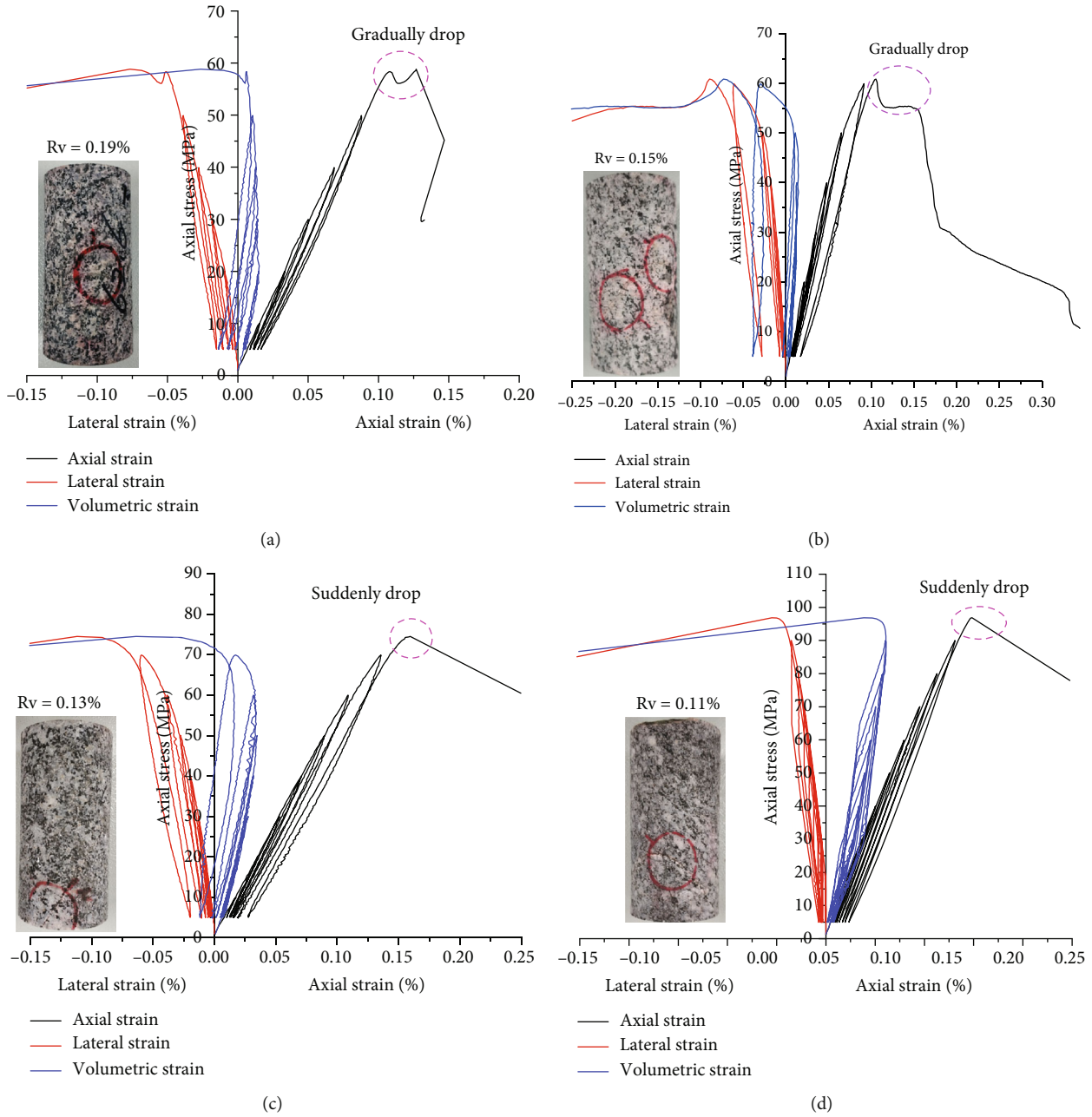

Figure 9: Axial stress strain curves for the samples experiencing different F-T cycles. (a–d) The natural fracture volume is 0.19%, 0.15%, 0.13%, and 0.11%, respectively.

samples. However, the volumetric strain as the combined effect of the axial and lateral strains decreases with increasing natural fracture scale. The change of volumetric deformation is the largest for the sample NFG-34 due to the larger preexisting fracture scale, and it is the minimum for the sample NGF-30.

3.4. Hysteresis Loop Pattern Analysis. During cyclic loading test, it can be seen that the reloading curve is not overlapped with the unloading curve, and a hysteresis loop forms on the stress strain curves. The unloading and reloading curves reflect the maximum elastic strain energy stored in a rock during a period. During unloading and reloading process, relative position among the unloading curve and the reloading curve has a significant influence on the area and shape of the hysteresis loop. The formation of a hysteresis loop reflects the plastic deformation inside rock, and its area reflects the dissipated energy within a cycle [26]. Two parameters of dynamic elastic modulus (E_d) and damping ratio (D_r) are usually used to evaluate the dissipated strain energy and the stored energy in a cycle. The result of these two parameters can be found in Meng [28] and Wang et al. [29]. The relationship between the dynamic elastic modulus and cycle number is plotted in Figures 12 and 13.

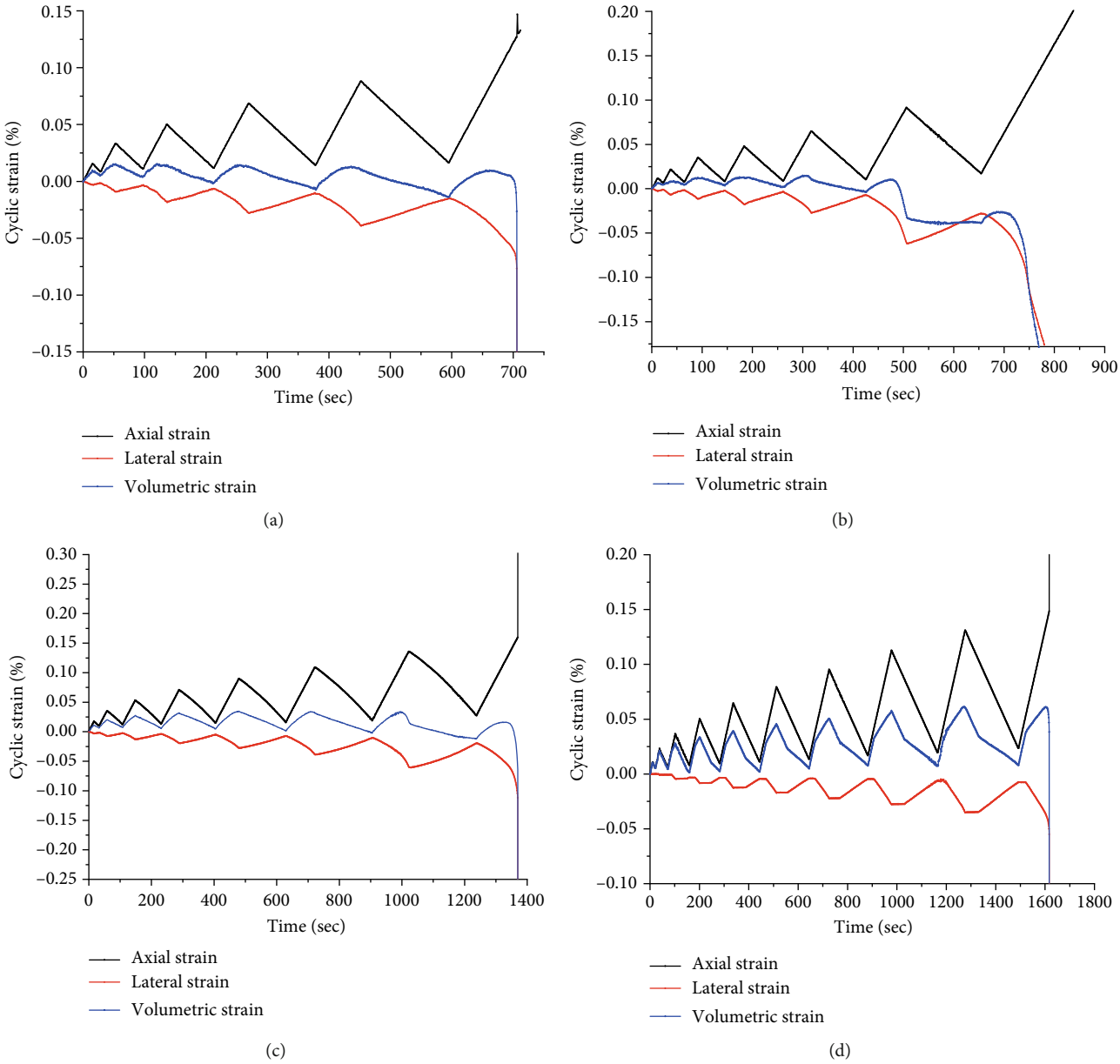

Figure 10: Plots of the (a) AE accumulative counts and the (b) AE accumulative energy against the freeze-thaw cycles.

In Figure 12, the dynamic elastic modulus first increases and then decreases with increasing cycle number; however, the onset of decrement is different. For the samples NFG-34 and NFG-14, the decreasing onset of M_r is earlier than the other two samples. This result reflects the decrement of sample stiffness and influenced by the natural fracture volume. For sample NFG-30, M_r is larger than other samples, and its stiffness gets to improve during cyclic loading. Figure 13 shows the evolution of damping ratio with cycle number. For all the tested samples, the damping ratio first decreases and then increases with increasing cycle number. Under low stress level, the cyclic stress results in the occurrence of reinforcement effect; therefore, damping ratio decreases with the cycle number. Under high stress level, crack initiation, and propagation in the sample, the rock structure is strongly deteriorated and damping ratio increases with the cycle number. It also can be seen that the inflection point on the damping ratio curve is different due to the existing of the natural fracture. When the natural fracture volume is relatively high (i.e., sample NFG-34), the onset of crack damage is earlier than other samples, and the moment of damping ratio increment is earlier than other cases. From these two figures, we can see that the changes of dynamic elastic modulus and damping ratio against cycle number are approximately opposite; these two parameters reflect the energy dissipation characteristics of rock during cyclic loading conditions. Taking the sample having the least natural fracture volume for example (i.e., NFG-30), it can be observed that the inflection point at the damping curve is earlier than the dynamic elastic modulus, indicating that the

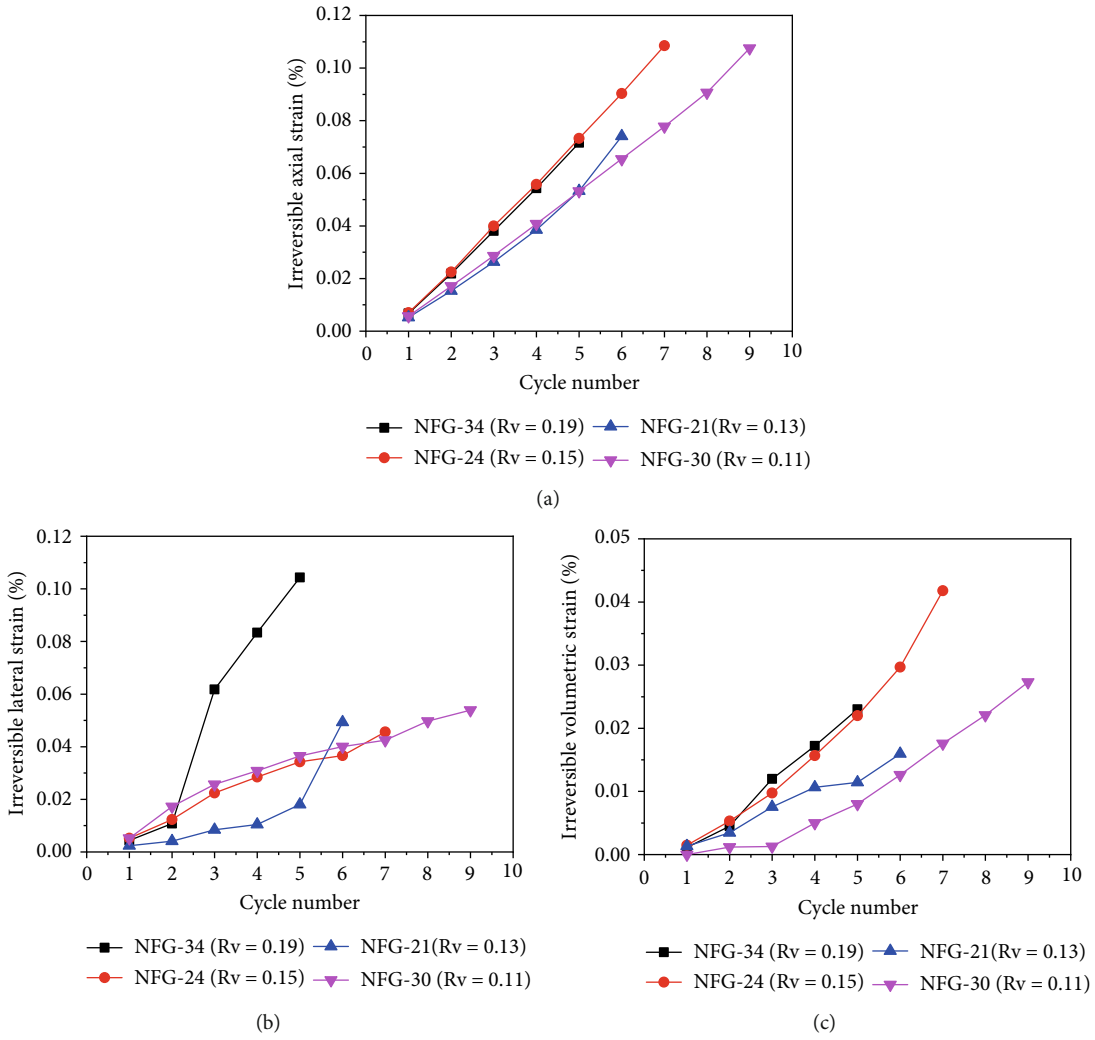

Figure 11: Plots of the irreversible deformation against the number of loading cycle. (a–c) Evolution of the axial, lateral, and volumetric irreversible strains with cycle loading number, respectively.

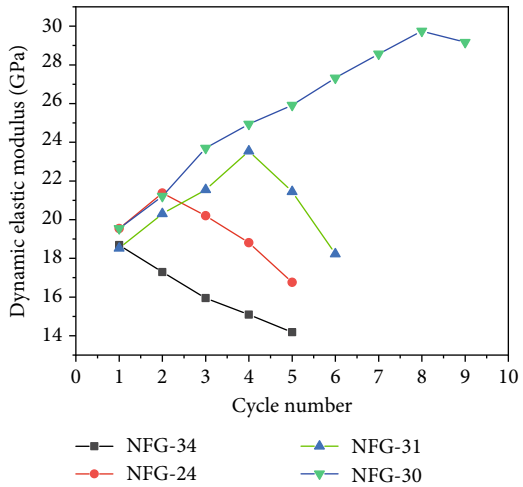

Figure 12: Evolution of dynamic elastic modulus with cycle number.

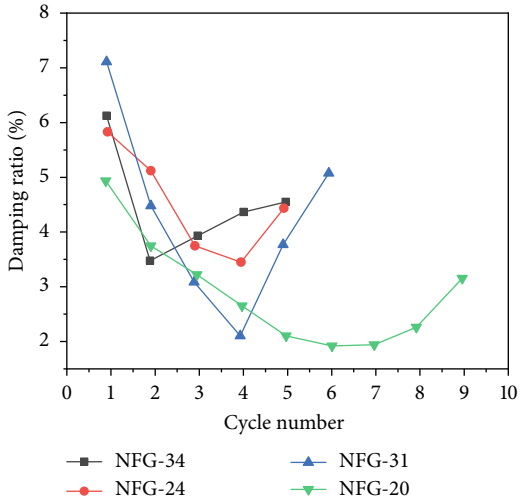

Figure 13: Evolution of dampling ratio with cycle number.

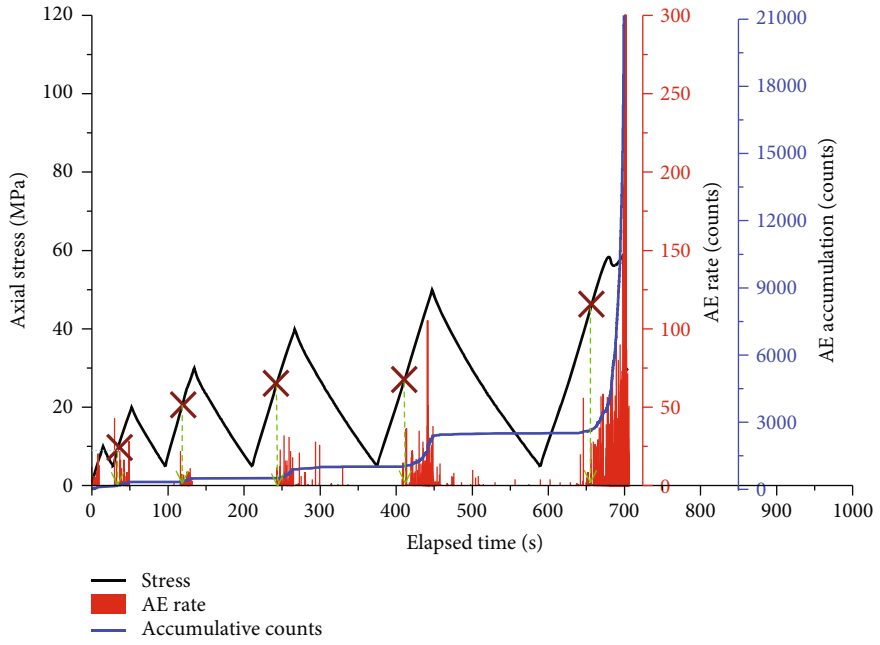

(a)

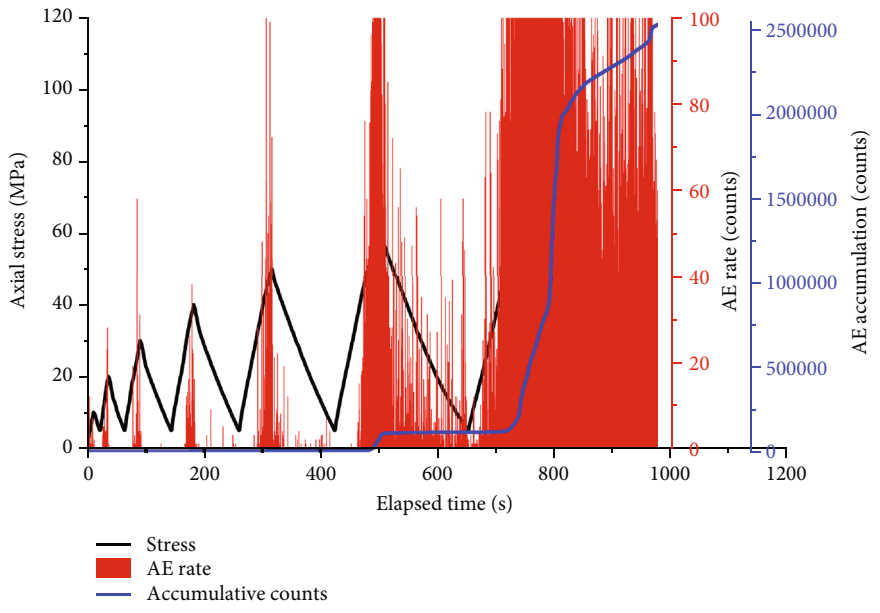

(b)

Figure 14: Continued.

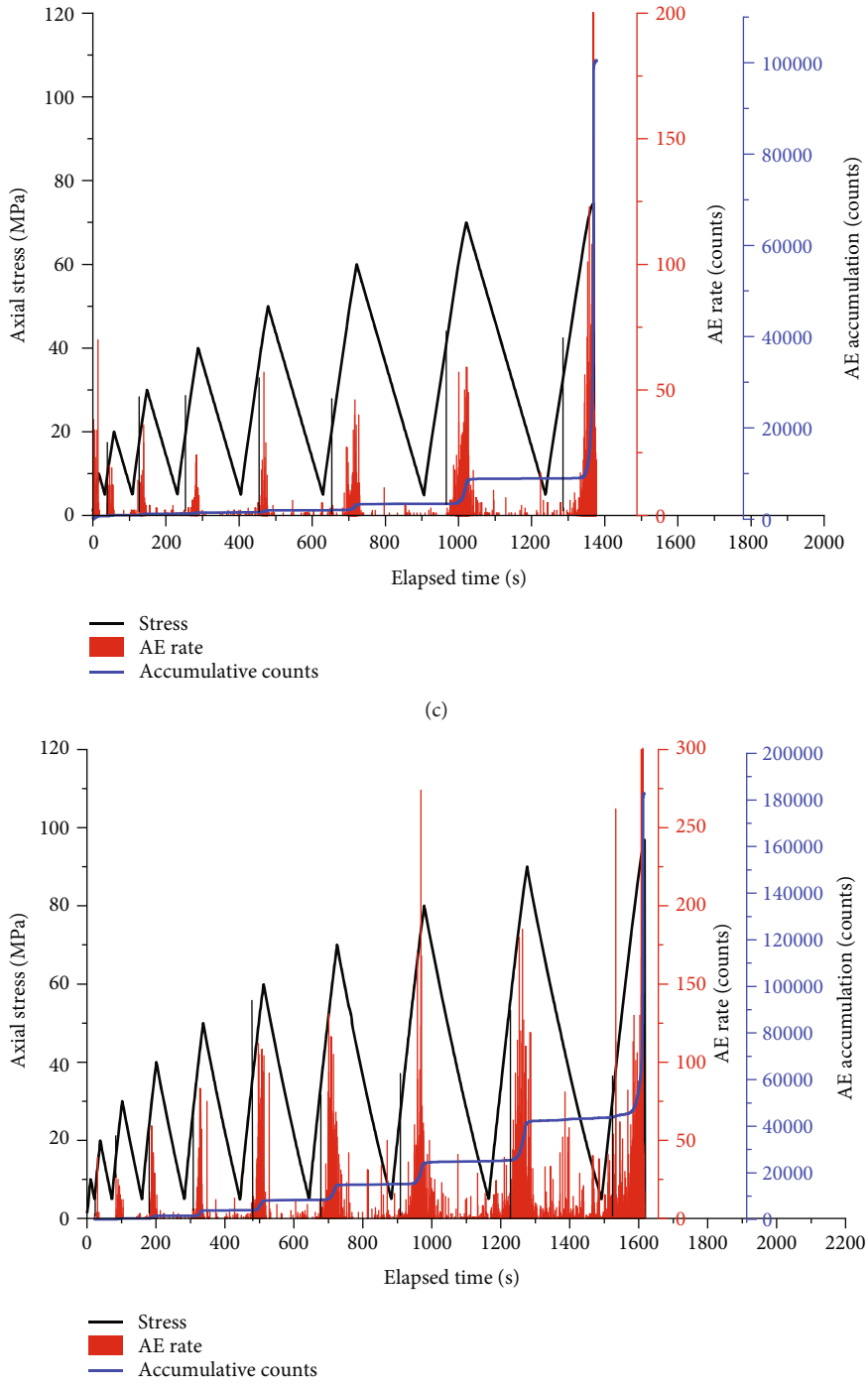

Figure 14: Output of AE counts for the tested granite samples. (a–d) It corresponds to samples of NFG-34, NFG-24, NFG-21, and NFG-30, and the corresponding natural fracture volume ratios are 0.19%, 0.15%, 0.13%, and 0.11%, respectively.

damping characteristics to cyclic loading are much more sensitive than the deformation modulus.

3.5. AE Count and Energy Analysis. The AE output from the four experiments as plotted against stress and time in Figures 14 and 15. During most cycles, the output of AE recommenced on any loading cycle at different stress levels that it ceased during the unloading portion of the previous cycle. The skip time of AE output curves is in consistent with the loading cycles, and AE output curves skip when the loading goes to the next cycle. The generation of AE counts in Figure 14 indicates the damage of mesostructures inside rock sample, and the damage gradually increases with loading cycles. It can be seen that the AE count increases with

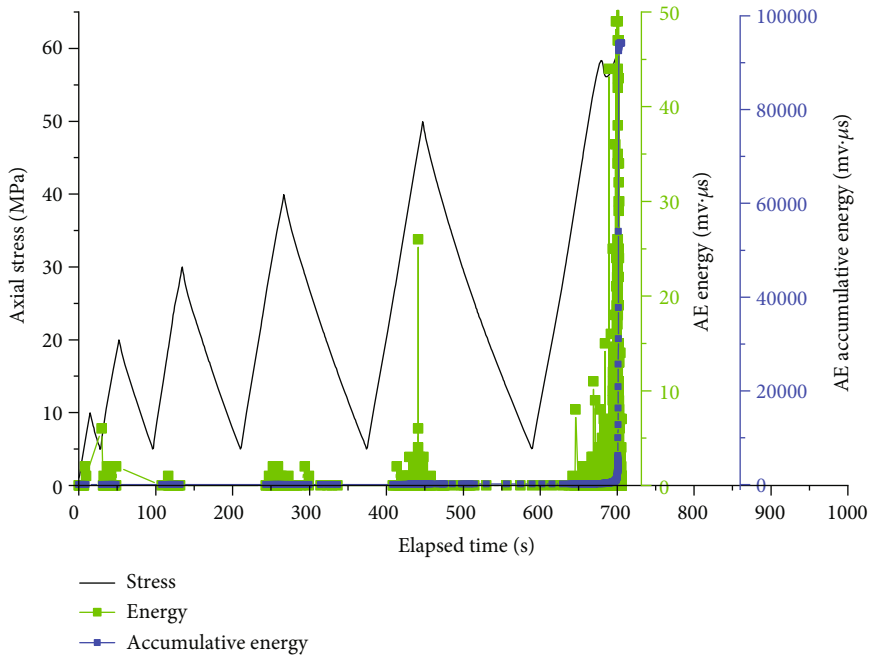

(a)

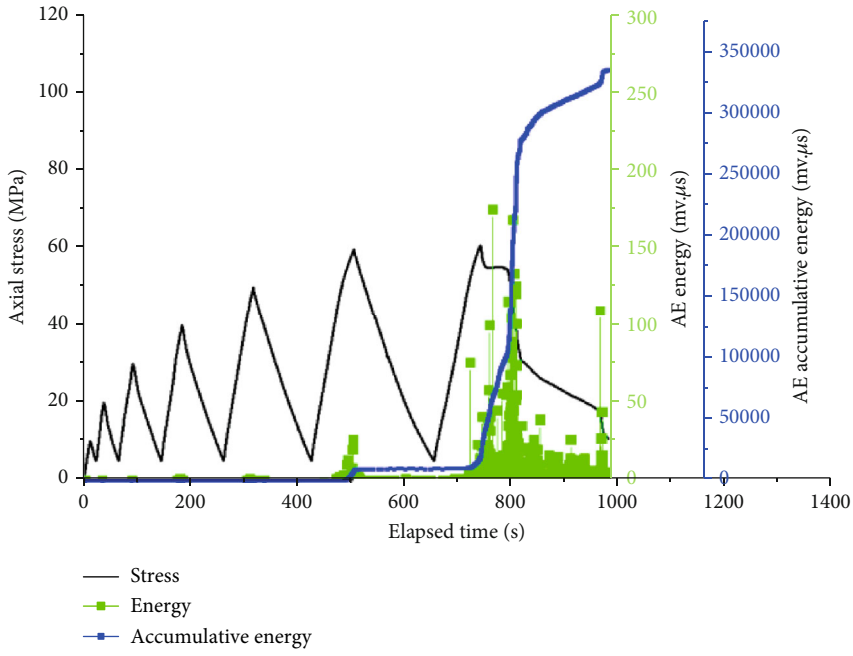

(b)

Figure 15: Continued.

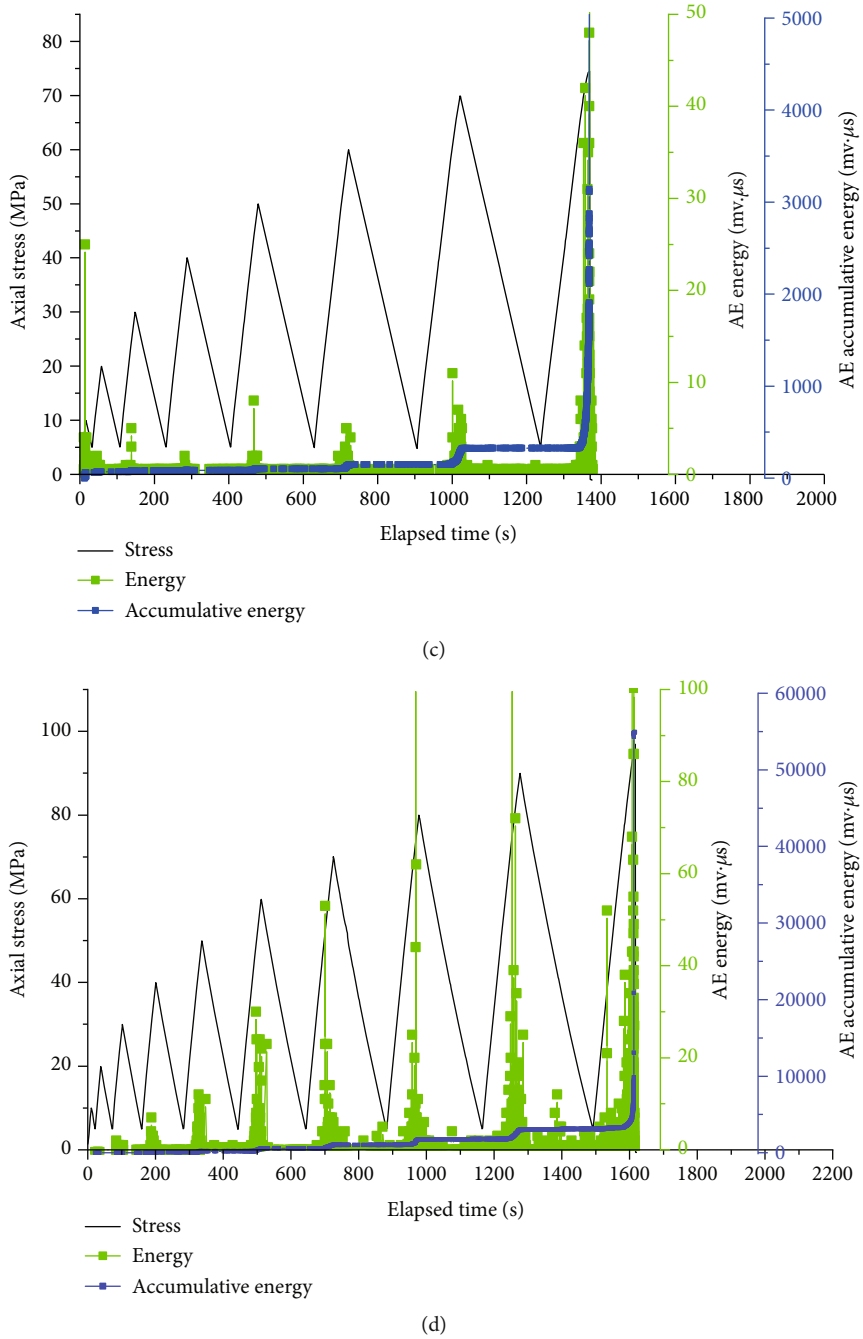

Figure 15: Output of AE energy for the tested granite samples. (a–d) It corresponds to samples of NFG-34, NFG-24, NFG-21, and NFG-30, and the corresponding natural fracture volume ratios are 0.19%, 0.15%, 0.13%, and 0.11%, respectively.

experimental time, and this reflects the deterioration of rock structure. We also note that the amount of AE counts/energy emitted during the final loading cycle, where microcracks link and coalesce to produce macroscopic failure of the sample, was much greater than for any of the previous cycles. Compared to the AE output pattern for the four tested samples, it can be found that the AE activities are different, especially at the failure stage. Taking the AE count curves for example, large amount of AE counts are recorded at the last cycle stage for the samples NFG-34 and NFG-24, and the AE count appears intensively. However, the appearance of AE counts is not so intensive for the samples NFG-21 and NFG-30. For the naturally fractured rock, the generation of AE counts is not attributed to the fracturing of rock (e.g., transgranular failure and intergranular failure), but also to the propagation of the preexisting fracture. For the samples NFG-34 and NFG-24, the scale of the preexisting fracture is relatively large, and AE counts resulting from the shearing sliding of the fractures are in the majority. For the sample NFG-24, the shear sliding at the preexisting fracture is the most serious and the AE count surges at the failure point.

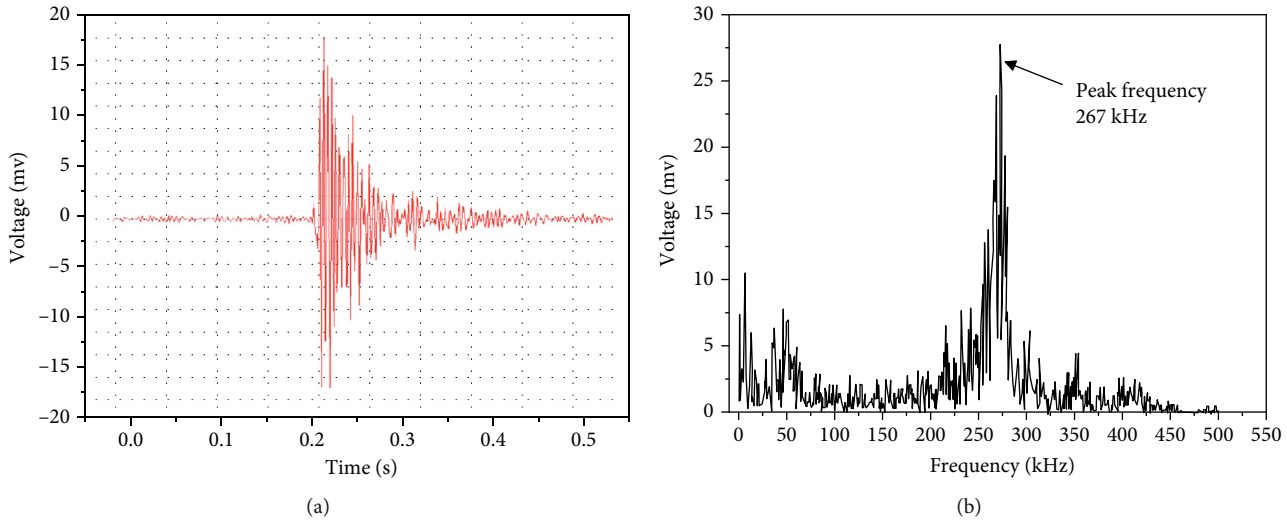

Figure 16: Frequency domain signal treatment to obtain the peak frequency of a fracturing event. (a) Original waveform of an AE event. (b) Plot of frequency against voltage to obtain the main frequency.

For the changes of AE energy against stress and time in Figure 15, similar conclusions can also be drawn. Because the AE energy is sensitive to the amplitude as well as the time duration, and it is less dependent on the operating frequencies and voltage threshold; this parameter is usually preferred for interpreting the magnitude of the source event over AE counts [27], and it can better reflect the crack initiation, propagation, and coalescence. It shows that the AE energy curve skips at the reloading stage, and the loading stress corresponding to the skip moment is not always increasing. The skip time is not only related to the new crack initiation but also the preexisting fractures. For the samples NFG-34 and NFG-24, we can observe that AE energy suddenly increases and the energy is the largest at the failure moment. This result indicates that failure of rock is along the preexisting fracture, and the shear-sliding failure occurs.

3.6. AE Spectrum Frequency Characteristics. The AE signals are consisted of a variety of frequency components, and the waveform frequency and amplitude are different for different AE sources [30–32]. The waveform characterization can reflect the crack type, number, and scale; therefore, the spectrum (frequency) information can well reflect the fracture process of rock. Existing research results have shown that the AE main frequency characteristics can better reflect the microfracturing of rock, and it is much more sensitive to the AE counts [27]. Different damage modes have been found to release AE signals with different frequency characteristics. Investigation of the frequency characteristics of emission events, on which our attention will be focused in this section, could be significant and promising as a mean of characterizing the effects of the preexisting natural fracture on fracturing process. By using fast Fourier transform (FFT) algorithm transformation, the extracted discrete time domain signal can be transferred to continuous frequency domain signal [4, 33]. Taking the rock sample of NFG-34 for example, the result of the peak frequency for a typical AE signal is plotted in Figure 16.

Using FFT method, the main frequency distribution during the rock deformation is shown in Figure 17. It can be seen that the low frequency, median frequency, and high frequency AE signals were recorded. Affected by the preexisting natural fracture, the frequency distribution is different due to the differential natural fracture volume. Table 2 lists the results of frequency spectrum characteristics for the four tested samples. At the initial loading stage, due to the close of the natural fracture and the consolidation of the rock matrix, friction-type AE signals were recorded and they have lower main frequency. With the increase of loading cycles, rock begins to damage and cracks initiate and propagate. The new cracks not only include the propagation of the natural fracture but also the new stimulated fracture in rock matrix. At this stage, fracture-type AE signals play a dominant role. At this time, the main frequency increases with the increase of loading cycles.

As is known, the AE studies on the fracture process of rock material have shown the stress waves in the form of acoustic emission (AE) signals that can give insights into the process of energy dissipation and release in response to the crack initiation and propagation. There is an inverse relationship between the AE frequency and the crack size. Generally, large-scaled cracks correspond to low frequency signals, and small-scaled cracks correspond to high frequency signals. The AE frequency band distribution indicates the mesoscopic fracturing mechanism of rock. In Table 2, it can be seen that the interval of low frequency band for the samples NFG-34, NFG-24, and NFG-21 is larger than the NFG-30; this result indicates that the overall fracture scale is relatively small. To quantificationally analyze the proportion of the three kinds of AE signals that occurs during rock fracturing, Table 3 roughly counts the percentage of the low, medium, and high frequency signals. The percentage of low frequency signals decreases and increases for the high frequency signals. This phenomenon can be also observed from Figure 17; at the last two cycles, the low frequency signals take the majority. The cracks at the last cycles are the

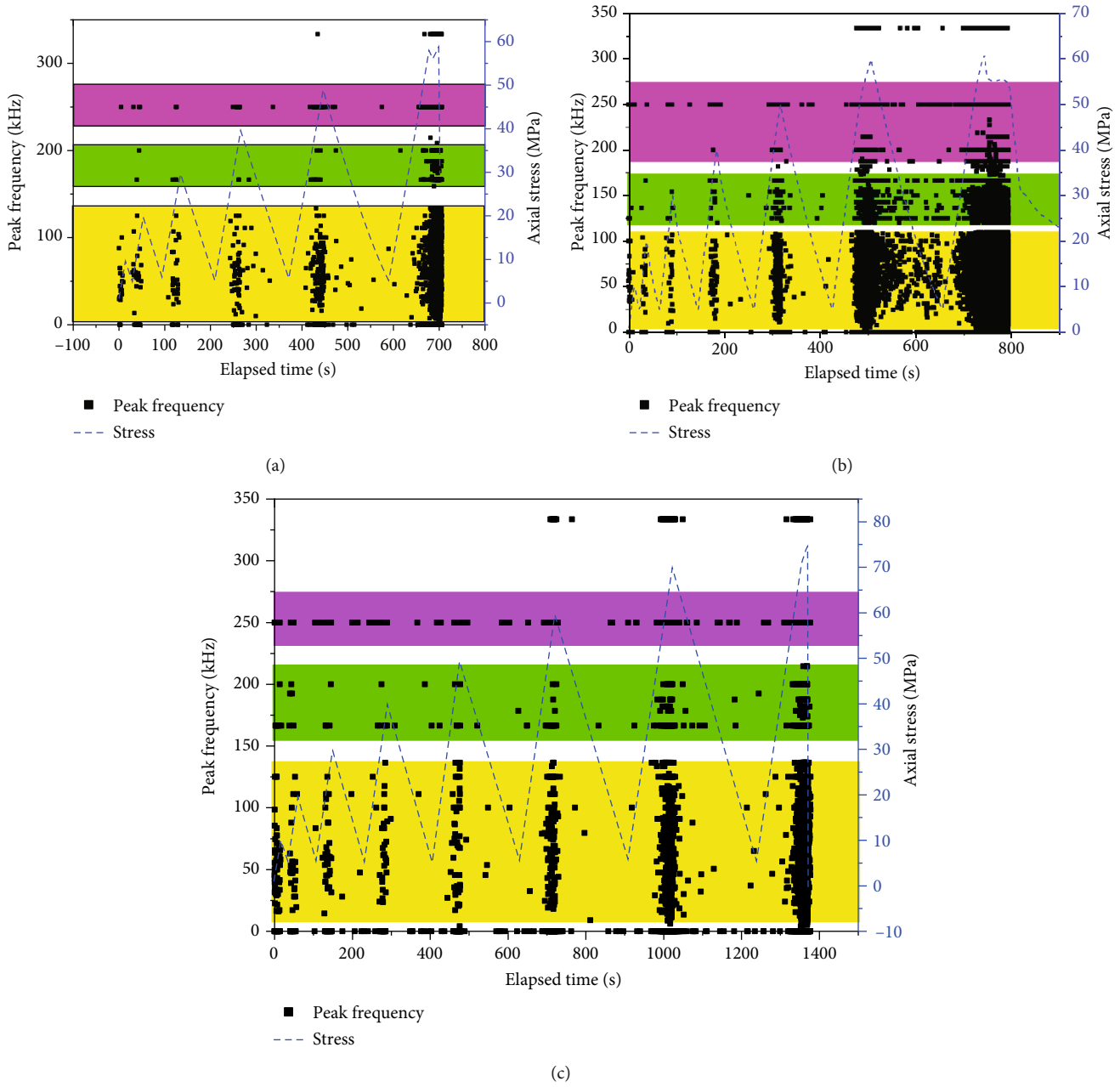

Figure 17: Continued.

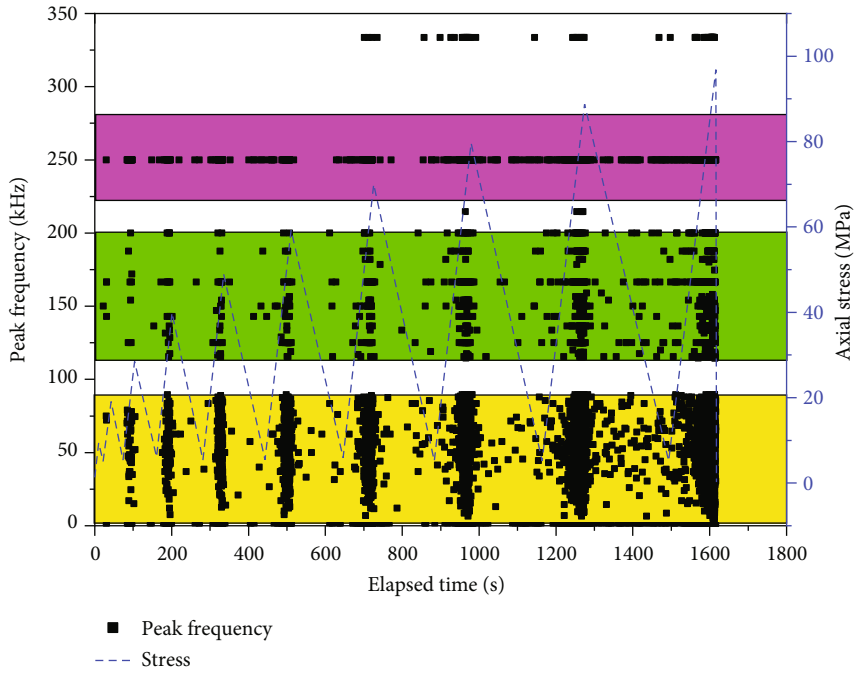

(d)

Figure 17: The main frequency characteristics of the tested samples during fracturing. (a–d) The sample IDs are NFG-34, NFG-24, NFG-21, and NFG-30, respectively. The corresponding natural fracture volume ratios are 0.19%, 0.15%, 0.13%, and 0.11%, respectively.

Table 2: Frequency spectrum characteristics of the tested granite sample during whole fracture process.

Sample ID	Initial damage degree (%)	Low frequency (kHz)	Median frequency (kHz)	High frequency (kHz)
NFG-34	0.19%	(5,135)	(160,210)	(245,255)
NFG-24	0.15%	(5,135)	(106,208)	(245,255)
NFG-21	0.13%	(5,135)	(155,210)	(245,255)
NFG-30	0.11%	(0,90)	(110,200)	(245,255)

Table 3: Percentage of the low, medium, and high frequency AE signals during rock deformation for the typical samples.

Sample ID	Initial damage degree (%)	Ratio of low frequency (%)	Ratio of median frequency (%)	Ratio of high frequency (%)
NFG-34	0.19%	64%	26%	10%
NFG-24	0.15%	70%	18%	12%
NFG-21	0.13%	51%	30%	19%
NFG-30	0.11%	45%	24%	31%

shear-type crack, which are almost shear sliding along the natural fractures, and the crack scale is large. The stress strain curves and AE counts/energy pattern can also prove this result. For the sample NFG-30, fractures are stimulated in the rock matrix and the brittle failure results in the occurrence of small-medium-scaled cracks. In addition, the energy releases are large when cracking occurs in the rock matrix, and the fracture-type AE signals have the high frequency characteristics.

3.7. Felicity Effect Analysis. For the increasing amplitude stress-cycling loading tests, AE output almost occurs when the loading goes to the next cycle, and the AE event intensifies before the previous maximum load. This phenomenon is the famous Felicity effect [34, 35]. The basic principle of Felicity effect is different from Kaiser effect, and the principle of Kaiser effect states that a material emits a noticeable AE when the reload stress exceeds the previously applied stress [35–38], and it reflects the stress memory. However, by contrast, for the Felicity effect, the AE becomes intensive before the previous maximum loading. The Felicity effect is usually associated to the stress path of cyclic loading and unloading. The associated quantitative measure of the effect is known as the Felicity ratio (FR), which is the ratio between the AE onset stress and the AE maximum of the previous stress, reflecting the development of previous damage and the structural defects of the material. According to the definition of FR of stress, the deformation characteristics of axial strain,

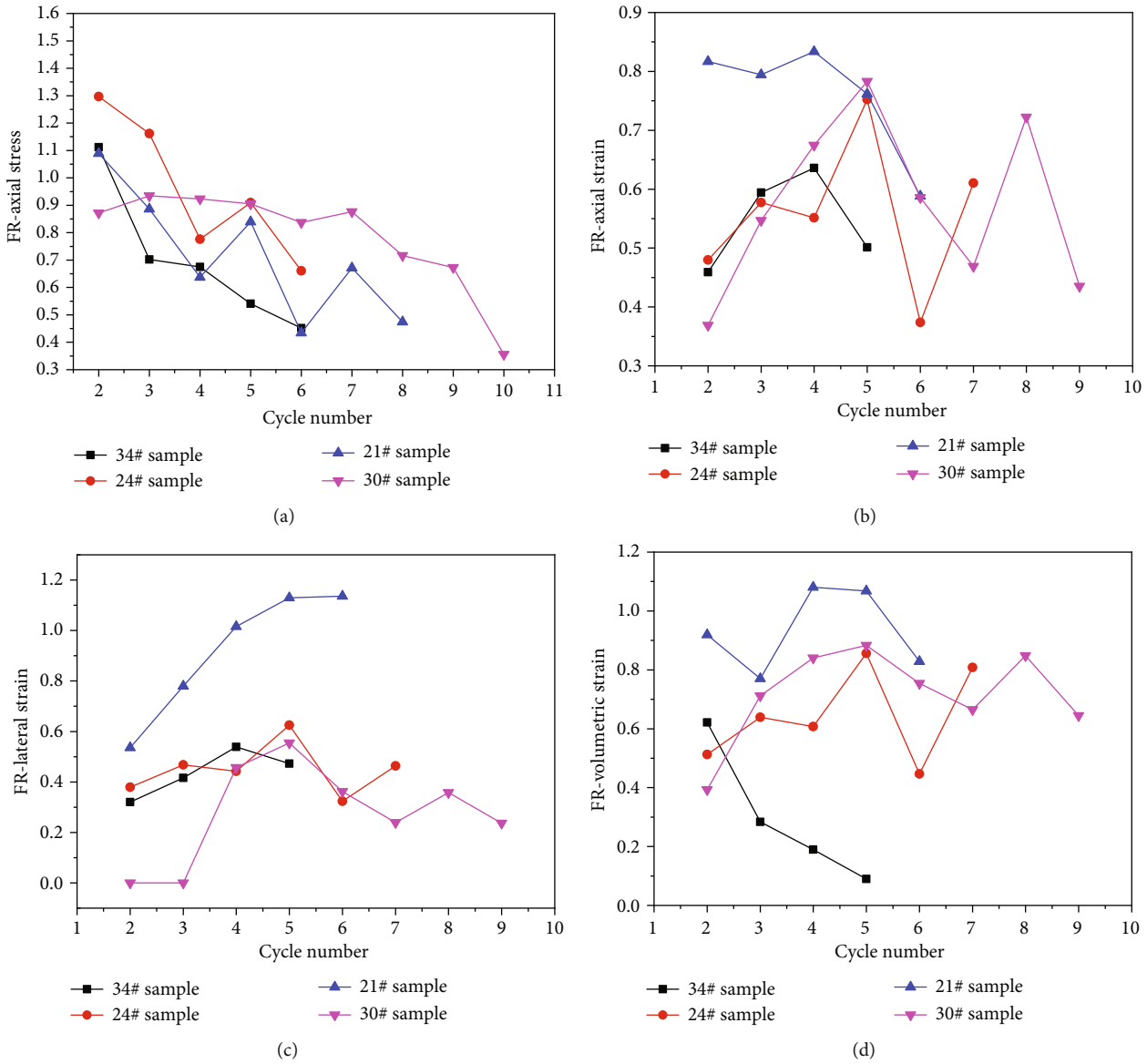

Figure 18: The main frequency characteristics of the tested samples during fracturing. (a–d) The sample IDs are NFG-34, NFG-24, NFG-21, and NFG-30, respectively. The corresponding natural fracture volume ratios are 0.19%, 0.15%, 0.13%, and 0.11%, respectively.

lateral strain, and volumetric strain are also expressed related to FR concept, and the expressions are as follows:

$$\mathrm{FR}_i = \frac{\sigma_i^{\mathrm{AE}}}{\sigma_{i-1}^{\mathrm{AE}}}, \tag{1}$$

$$\mathrm{FR}(\varepsilon_a)_i = \frac{(\varepsilon_a)_i^{\mathrm{AE}}}{(\varepsilon_a)_{i-1}^{\mathrm{AE}}}, \tag{2}$$

$$\mathrm{FR}(\varepsilon_l)_i = \frac{(\varepsilon_l)_i^{\mathrm{AE}}}{(\varepsilon_l)_{i-1}^{\mathrm{AE}}}, \tag{3}$$

$$\mathrm{FR}(\varepsilon_v)_i = \frac{(\varepsilon_v)_i^{\mathrm{AE}}}{(\varepsilon_v)_{i-1}^{\mathrm{AE}}}, \tag{4}$$

where FR_i is the definition of the Felicity ratio in the i^{th} cycle. $(\varepsilon_a)_i^{\mathrm{AE}}$, $(\varepsilon_l)_i^{\mathrm{AE}}$, and $(\varepsilon_v)_i^{\mathrm{AE}}$ are the axial, lateral, and volumetric strains corresponding to the AE generation at the i^{th} cycle, respectively; $(\varepsilon_a)_{i-1}^{\mathrm{AE}}$, $(\varepsilon_l)_{i-1}^{\mathrm{AE}}$, and $(\varepsilon_v)_{i-1}^{\mathrm{AE}}$ are the maximum axial, lateral, and volumetric strains in the $i-1^{\mathrm{th}}$ cycle, respectively.

The FR of the axial stress and the various deformation characteristics against cycle number is shown in Figure 18. For the tested rock, the Felicity effect is strongly impacted by the preexisting natural fractures, and the fracture volume influences the damage evolution. In Figure 18(a), for the samples NFG-34, NFG-24, and NFG-21, at the initial three cyclic loading, FR > 1, and obvious Kaiser effect occurs; after the three cyclic loading and unloading, FR < 1, and the Felicity effect is obvious, and Kaiser effect disappears accordingly.

However, for the sample NFG-30, FR < 1, during the whole deformation. It indicates that the rock damage of NFG-30 with larger natural fractures is relatively serious, and crack begins to form and propagate until failure of the rock sample. For NFG-30, the Felicity ratio is less than 1 after the three cycles until rock failure. Affected by the rock structure, the changes of FR show different evolution patterns, and a monotonous decreasing trend is for the sample NFG-24, and fluctuation decreasing trend is for the samples NFG-34, NFG-21, and NFG-30. In Figures 18(b)–18(d), the FR of the axial, lateral, and volumetric deformations presents as fluctuation trend; this indicates the influence of preexisting natural fracture on rock deformation and the associated AE pattern; the existing of natural fracture alters the fracture propagation path, and the interactions between natural fracture and the newly stimulated fracture result in complicated fracturing behaviors. The compaction of the natural fracture and the formation of new cracks influence the deformation characteristics. Our results for the rock sample containing preexisting natural fractures are different from the experimental results of intact rock reported by Wang et al. [33] and Kaiser [36].

4. Discussions

Although plenty of previous works have been done on rock material to reveal the impact of F-T on its physical and mechanical properties, most of the studies were performed on intact rock [2–4]. The frost heaving pressure is mainly acted on the pores, and damage occurs among rock mineral boundaries. Different to the previous studies, granite samples obtained from an open pit mining slope with a group of dominant structural plane are experimentally studied. The natural fracture volume not only affects the mechanical behavior but also the AE pattern. The previous studies have shown that the mesoscopic structural changes of rock impact its whole mechanical behaviors [39–45]. This work further indicates the structural dependence of rock mechanical and AE characteristics for rock subjected to cyclic loads. Under F-T treatment, the frost heaving pressure in the structural plane is larger enough to drive the crack propagation and the failure of rock. For the naturally fractured rock, repeated freeze-thaw action impacts the evolution of fracture aperture. The evolution law of aperture is related to the fracture opening and filling degree.

Water migration and water-ice phase transformation in natural fractures accelerate the deterioration of rock mesostructure and the associated mechanical and AE pattern [4, 27]. Different AE counts/energy responses have been recorded, and the crack initiation and propagation at the preexisting facture and the rock matrix have different AE patterns. For the samples NFG-34 and NFG-24 having relatively high natural fracture volume, the shear sliding on the natural fracture is obvious and the energy release is smaller than the samples NFG-21 and NFG-30. The frequency spectrum analysis throws new insight on the fracture mechanism of rock. Low frequency signals play a dominant role during rock fracturing process, especially at the failure stage, and plenty of low frequency signals occur which reflect the block sliding along the natural fracture.

The Felicity effect reflects the stress memory of rock. Owing to the existing of natural fractures in rock, the Felicity effect can be divided into two parts: in the former cycle, friction-type AE signals occur resulting from frictionally sliding on the preexisting natural fractures, and the weak and sparse AE activities with low energy occur because of the breakage of asperities on the original fracture surface; in the latter cycle, stress redistributed and new fracture forms because of the fracturing into rock matrix or the propagation of the preexisting fracture, and continuous and strong AE activities generate. The preloading has important impact on the stress memory of crack. Due to the existing of natural fractures, the volumetric dilation of rock was much more obvious than those intact rock samples, and it can be easily to get the Felicity effect when the preloading stress exceeds the crack dilation stress. The irreversible volumetric deformation results in the aggravation of rock damage, and the Felicity effect becomes more and more obvious. Owing to the interaction between the preexisting fractures and the new stimulated fracture, the AE-recovered stress at the reloading is not always small than the previous stress; therefore, the curve of the Felicity ratio against cycle number presents as fluctuation trend. This phenomenon is different from the intact rock. For intact rock, the failure has progressive pattern, and the crack initiation and propagation occur when the reloaded stress exceeds the preloading stress, and Felicity ratio usually shows monotonous decreasing trend.

5. Conclusions

To investigate the impacts of the preexisting natural fracture on the mechanical and acoustic emission characteristics of hard rock samples after F-T treatment, cyclic loading test combined with in situ AE monitoring technique was carried out on naturally fractured granite samples cored from an open pit mine slope located in the Hejing country, Xinjiang province. Some main conclusions can be summarized from the present study:

(1) During cyclic F-T treatment, frost heaving pressure generates and acts on the natural fractures, and the fracture aperture changes with increasing F-T cycle. The relations between the fracture aperture and F-T number are impacted by fracture openness and fill condition. The increasing rate of fractyre aperture is the largest for the open-type natural fracture

(2) The preexisting natural fracture impacts the strength, deformation, AE pattern, and the Felicity effect. The interactions between the stimulated natural fracture and the newly formed fractures are the basic reason resulting in the different responses of AE actives during cyclic loading. The proportion of AE signals having low frequency characteristics decreases with increasing natural fracture volume. This indicates the formation of large-scaled fracture during sample deformation, and it is related to the shear sliding of the preexisting natural fracture

(3) The Felicity effect observed for the tested samples indicates that FR presents fluctuation decreasing trend that is different from the intact rock. FR shows obvious dependence on the preexisting natural fracture. The rock internal structure is much more nonhomogeneity when having high natural fracture volume, and this causes the earliest onset of AE activities and lowest FR

Data Availability

The experimental data used to support the findings of this study are included within the article.

Conflicts of Interest

The authors declare no conflict of interest.

Acknowledgments

The authors would like to thank the editors and the anonymous reviewers for their helpful and constructive comments. This research was funded by the Beijing Natural Science Foundation (8202033), the National Key Technologies Research and Development Program (2018YFC0808402), the Fundamental Research Funds for the Central Universities (FRF-TP-20-004A2 and 06500072), the National Natural Science Foundation of China (51774021), the Natural Science Foundation of Guizhou Province ([2019]1169), and Guizhou Education Department Foundation for Youth ([2018]151).

References

[1] D. P. Halsey, D. J. Mitchell, and S. J. Dews, "Influence of climatically induced cycles in physical weathering," *Quarterly Journal of Engineering Geology and Hydrogeology*, vol. 31, no. 4, pp. 359–367, 1998.

[2] N. Matsuoka, "Microgelivation versus macrogelivation: towards bridging the gap between laboratory and field frost weathering," *Permafrost and Periglacial Processes*, vol. 12, no. 3, pp. 299–313, 2001.

[3] M. Takarli, W. Prince, and R. Siddique, "Damage in granite under heating/cooling cycles and water freeze - thaw condition," *International Journal of Rock Mechanics and Mining Sciences*, vol. 45, no. 7, pp. 1164–1175, 2008.

[4] Y. Wang, W. K. Feng, H. J. Wang, C. H. Li, and Z. Q. Hou, "Rock bridge fracturing characteristics in granite induced by freeze-thaw and uniaxial deformation revealed by AE monitoring and post-test CT scanning," *Cold Regions Science and Technology*, vol. 177, article 103115, 2020.

[5] Y. Wang, B. Zhang, S. H. Gao, and C.H. Li, "Investigation on the effect of freeze-thaw on fracture mode classification in marble subjected to multi-level cyclic loads," *Theoretical and Applied Fracture Mechanics*, vol. 11, article 102847, 2020.

[6] M. Hori and H. Morihiro, "Micromechanical analysis on deterioration due to freezing and thawing in porous brittle materials," *International Journal of Engineering Science*, vol. 36, no. 4, pp. 511–522, 1998.

[7] D. T. Nicholson and F. H. Nicholson, "Physical deterioration of sedimentary rocks subjected to experimental freeze–thaw weathering," *Earth Surface Processes and Landformss*, vol. 25, no. 12, pp. 1295–1307, 2000.

[8] Y. Wang, J. Q. Han, and C. H. Li, "Acoustic emission and CT investigation on fracture evolution of granite containing two flaws subjected to freeze–thaw and cyclic uniaxial increasing-amplitude loading conditions," *Construction and Building Materials*, vol. 260, p. 119769, 2020.

[9] L. P. Zhu, W. B. Whalleyz, and J. C. Wang, "A simulated weathering experiment of small free granite blocks under freeze–thaw conditions," *Journal of Glaciology and Geocryology*, vol. 19, no. 4, pp. 302–310, 1997.

[10] S. J. Chen, D. W. Yin, N. Jiang, F. Wang, and Z. Zhao, "Mechanical properties of oil shale-coal composite samples," *International Journal of Rock Mechanics and Mining Sciences*, vol. 123, p. 104120, 2019.

[11] J. Park, C. U. Hyun, and H. D. Park, "Changes in microstructure and physical properties of rocks caused by artificial freeze–thaw action," *Bulletin of Engineering Geology and the Environment*, vol. 74, no. 2, pp. 555–565, 2015.

[12] T. C. Chen, M. R. Yeung, and N. Mori, "Effect of water saturation on deterioration of welded tuff due to freeze–thaw action," *Cold Regions Science and Technology*, vol. 38, no. 2-3, pp. 127–136, 2004.

[13] B. Ke, K. Zhou, C. Xu, H. Deng, J. Li, and F. Bin, "Dynamic mechanical property deterioration model of sandstone caused by freeze–thaw weathering," *Rock Mechanics and Rock Engineering*, vol. 51, no. 9, pp. 2791–2804, 2018.

[14] X. Fang, J. Xu, and P. Wang, "Compressive failure characteristics of yellow sandstone subjected to the coupling effects of chemical corrosion and repeated freezing and thawing," *Engineering Geology*, vol. 233, pp. 160–171, 2018.

[15] L. Qin, C. Zhai, S. Liu, J. Xu, G. Yu, and Y. Sun, "Changes in the petrophysical properties of coal subjected to liquid nitrogen freeze-thaw–a nuclear magnetic resonance investigation," *Fuel*, vol. 194, pp. 102–114, 2017.

[16] L. W. Kong, Z. X. Zeng, W. Bai, and M. Wang, "Engineering geological properties of weathered swelling mudstones and their effects on the landslides occurrence in the Yanji section of the Jilin-Hunchun high-speed railway," *Bulletin of Engineering Geology and the Environment*, vol. 77, no. 4, pp. 1491–1503, 2018.

[17] Q. Ma, D. Ma, and Z. Yao, "Influence of freeze-thaw cycles on dynamic compressive strength and energy distribution of soft rock specimen," *Cold Regions Science and Technology*, vol. 153, pp. 10–17, 2018.

[18] J. Zhang, H. Fu, Z. Huang, Y. Wu, W. Chen, and Y. Shi, "Experimental study on the tensile strength and failure characteristics of transversely isotropic rocks after freeze-thaw cycles," *Cold Regions Science and Technology*, vol. 163, pp. 68–77, 2019.

[19] S. B. Huang, Q. S. Liu, Y. Z. Liu, Y. S. Kang, A. P. Cheng, and Z. Y. Ye, "Frost heaving and frost cracking of elliptical cavities (fractures) in low-permeability rock," *Engineering Geology*, vol. 234, pp. 1–10, 2018.

[20] S. Huang, Q. Liu, A. Cheng, Y. Liu, and G. Liu, "A fully coupled thermo-hydro-mechanical model including the determination of coupling parameters for freezing rock," *International Journal of Rock Mechanics and Mining Sciences*, vol. 103, pp. 205–214, 2018.

[21] Y. Lu, X. Li, and A. Chan, "Damage constitutive model of single flaw sandstone under freeze-thaw and load," *Cold Regions Science and Technology*, vol. 159, pp. 20–28, 2019.

[22] X. P. Zhou, Y. Niu, J. Z. Zhang, X. C. Shen, Y. Zheng, and F. Berto, "Experimental study on effects of freeze-thaw fatigue damage on the cracking behaviors of sandstone containing two unparallel fissures," *Fatigue & Fracture of Engineering Materials & Structures*, vol. 42, no. 6, pp. 1322–1340, 2018.

[23] Y. Wang, S. H. Gao, C. H. Li, and J. Q. Han, "Investigation on fracture behaviors and damage evolution modeling of freeze-thawed marble subjected to increasing-amplitude cyclic loads," *Theoretical and Applied Fracture Mechanics*, vol. 109, article 102679, 2020.

[24] Y. Wang, W. K. Feng, and C. H. Li, "On anisotropic fracture and energy evolution of marble subjected to triaxial fatigue cyclic-confining pressure unloading conditions," *International Journal of Fatigue*, vol. 134, p. 105524, 2020.

[25] Y. Wang, S. Gao, D. Liu, and C. Li, "Anisotropic fatigue behaviour of interbeded marble subjected to uniaxial cyclic compressive loads," *Fatigue & Fracture of Engineering Materials & Structures*, vol. 43, no. 6, pp. 1170–1183, 2020.

[26] Y. Wang, C. Li, J. Han, and H. Wang, "Mechanical behaviours of granite containing two flaws under uniaxial increasing amplitude fatigue loading conditions: an insight into fracture evolution analyses," *Fatigue and Fracture of Engineering Materials and Structures*, vol. 43, no. 9, pp. 2055–2070, 2020.

[27] Y. Wang, C. H. Li, H. Liu, and J. Q. Han, "Fracture failure analysis of freeze–thawed granite containing natural fracture under uniaxial multi-level cyclic loads," *Theoretical and Applied Fracture Mechanics*, vol. 110, p. 102782, 2020.

[28] F. Y. Menq, *Dynamic properties of sandy and gravelly soils, [Ph.D. Thesis]*, The University of Texas at Austin, 2003.

[29] Y. Wang, X. M. Wei, and C. H. Li, "Dynamic behavior of soil and rock mixture using cyclic triaxial tests and X-ray computed tomography," *Arabian Journal of Geosciences*, vol. 12, no. 7, p. 229, 2019.

[30] M. Ohnaka and K. Mogi, "Frequency characteristics of acoustic emission in rocks under uniaxial compression and its relation to the fracturing process to failure," *Journal of geophysical research: Solid Earth*, vol. 87, no. B5, pp. 3873–3884, 1982.

[31] M. C. He, J. L. Miao, and J. L. Feng, "Rock burst process of limestone and its acoustic emission characteristics under true-triaxial unloading conditions," *International Journal of Rock Mechanics and Mining Sciences*, vol. 47, no. 2, pp. 286–298, 2010.

[32] Z. Wang, J. Ning, and H. Ren, "Frequency characteristics of the released stress wave by propagating cracks in brittle materials," *Theoretical and Applied Fracture Mechanics*, vol. 96, pp. 72–82, 2018.

[33] Y. Wang, S. H. Gao, C. H. Li, and J. Q. Han, "Energy dissipation and damage evolution for dynamic fracture of marble subjected to freeze-thaw and multiple level compressive fatigue loading," *International Journal of Fatigue*, vol. 142, article 105927, 2020.

[34] M. A. Hamstad, "Discussion of the basic understanding of the Felicity effect in fibre composites," *Journal of Acoustic Emission*, vol. 5, no. 2, pp. 95–102, 1986.

[35] Y. Zhang, Y. Chen, R. Yu, L. Hu, and M. Irfan, "Effect of loading rate on the felicity effect of three rock types," *Rock Mechanics and Rock Engineering*, vol. 50, no. 6, pp. 1673–1681, 2017.

[36] J. Kaiser, "Erkenntnisse und Folgerungen aus der Messung von Gerauschen bei Zugbeanspruchung von metallischen Werkstoffen," *Archiv für das Eisenhüttenwesen*, vol. 24, no. 1/2, pp. 43–45, 1953.

[37] A. Lehtonen, J. W. Cosgrove, J. A. Hudson, and E. Johansson, "An examination of in situ rock stress estimation using the Kaiser effect," *Engineering Geology*, vol. 124, pp. 24–37, 2012.

[38] D. Lockner, "The role of acoustic emission in the study of rock fracture," *International Journal of Rock Mechanics and Mining Sciences*, vol. 30, no. 7, pp. 883–899, 1993.

[39] Z. Li, H. Liu, Z. Dun, L. Ren, and J. Fang, "Grouting effect on rock fracture using shear and seepage assessment," *Construction and Building Materials*, vol. 242, article 118131, 2020.

[40] Z. Li, H. Zhou, D. Hu, and C. Zhang, "Yield criterion for rock-like geomaterials based on strain energy and CMP model," *International Journal of Geomechanics*, vol. 20, no. 3, article 04020013, 2020.

[41] Y. Wang, Y. Z. Hu, and S. H. Gao, "Dynamic mechanical behaviors of interbedded marble subjected to multi-level uniaxial compressive cyclic loading conditions: an insight into fracture evolution analysis," *Engineering Fracture Mechanics*, vol. 109, no. article 107410, 2020.

[42] X. Wang, C. Liu, S. Chen, L. Chen, K. Li, and N. Liu, "Impact of coal sector's de-capacity policy on coal price," *Applied Energy*, vol. 265, p. 114802, 2020.

[43] Y. Wang, D. Q. Liu, J. Q. Han, C. H. Li, and H. Liu, "Effect of fatigue loading-confining stress unloading rate on marble mechanical behaviors: an insight into fracture evolution analyses," *Journal of Rock Mechanics and Geotechnical Engineering*, vol. 12, 2020.

[44] Q. Meng, H. Wang, M. Cai, W. Xu, X. Zhuang, and T. Rabczuk, "Three-dimensional mesoscale computational modeling of soil-rock mixtures with concave particles," *Engineering Geology*, vol. 277, article 105802, 2020.

[45] Z. Li, S. Liu, W. Ren, J. Fang, Q. Zhu, and Z. Dun, "Multiscale laboratory study and numerical analysis of water-weakening effect on shale," *Advances in Materials Science and Engineering*, vol. 2020, Article ID 5263431, 14 pages, 2020.